Energy 252 (2022) 123909

Contents lists available at ScienceDirect

Energy

journal homepage: www.elsevier.com/locate/energy

Equation-oriented methods for optimizing Rankine cycles using radial inflow turbine

Brede A.L. Hagen [a, *], Trond Andresen [b], Petter Nekså [a, b]

[a] Department of Energy and Process Engineering, NTNU – Norwegian University of Science and Technology, Kolbjørn Hejes vei 1B, NO-7491, Trondheim, Norway
[b] SINTEF Energy Research, Norway

ARTICLE INFO

Article history:
Received 12 August 2021
Received in revised form
26 January 2022
Accepted 1 April 2022
Available online 26 April 2022

Keywords:
Gradient-based optimization
Mean-line model
Design
Off-design
Control approach

ABSTRACT

This paper presents methods for optimizing the design and the performance of Rankine cycles using radial inflow turbines. Both methods follow a novel equation-oriented approach and involve a single mathematical problem that is solved by an efficient gradient-based algorithm. The capabilities of the proposed methods were demonstrated through a case study for power generation from the batch-wise casting process at a representative ferroalloy plant. More specifically, the proposed methods were used to design and analyze three Rankine cycles with CO_2 as the working fluid. The design optimization method converged in most cases to essentially the same solution regardless of the start values of the independent variables. The performance optimization method demonstrated that the control approaches with variable rotational turbine speed improved the turbine off-design efficiency over the control approaches with a constant rotational speed. Moreover, the control approaches with variable inlet guide vanes improved the thermodynamic performance of the cycle by facilitating operation at a higher pressure than the control approaches with a fixed geometry turbine. Considering the flexibility, robustness and the computational cost of the proposed methods, they can be regarded as a powerful tool for the preliminary design and performance prediction of Rankine cycles.

1. Introduction

Increasing concerns of global warming due the emission of anthropogenic greenhouse gases has resulted in ambitious climate goals world-wide. For example, the European Union recently increased their ambition to reduce their greenhouse gas emissions by at least 55% within 2030 compared to the emission level in 1990 [1]. One key to reach this goal is to replace fossil energy, whose utilization emits the greenhouse gas CO_2, with more environmentally friendly heat sources for producing power. Examples of such energy sources are industrial surplus heat [2], biomass [3], solar energy [4] and geothermal energy [5]. These energy sources could provide a significant fraction of the worlds power demand [6], but their limited capacity and/or temperature constrain their widespread utilization. First, the use of steam Rankine cycle [7], is challenging for systems below a few MWe because the combination of small mass flow rate and large volume flow ratio lead to capital intensive expanders with low efficiency [8]. Although, the expander design challenge can be overcome by using an organic fluid [8,9] or CO_2 [10] as the working fluid, the low efficiencies associated with power production from low temperature heat sources is a challenge for the profitability of any Rankine cycle system. Therefore, a key factor to enable further utilization of environmentally friendly heat sources for power production, is to increase the cost-effectiveness of Rankine cycle systems.

One way to achieve this in applications for which the heat source or sink characteristics vary with time is to account for the off-design performance of the system during the design phase. For instance, Capra and Martelli [11] demonstrated that a design optimization that takes into account the off-design performance of the Rankine cycle can significantly increase the cost-effectiveness of the system with respect to a conventional design approach that only accounts for the system performance at the nominal operating point. More specifically, Capra and Martelli [11] applied the two aforementioned methods to design a combined heat and power Rankine cycle and showed that the former resulted in up to 22% higher annual profit than the latter [12].

In addition, the efficiency of Rankine cycle systems whose

* Corresponding author.
E-mail address: brede.hagen@ntnu.no (B.A.L. Hagen).

https://doi.org/10.1016/j.energy.2022.123909

Nomenclature

Roman symbols

A_c	Cross-sectional flow area [m^2]
A_s	Heat transfer surface area [m^2]
A_5	Rotor throat area [m^2]
D_h	Hydraulic diameter [m]
L	Heat exchanger length [m]
h	Specific enthalpy [J/kg]
$\dot{m}$	Mass flow rate [kg/s]
o_n	Nozzle throat opening [m]
p	Pressure [Pa]
$P = 4A_c/D_h$	Channel perimeter [m]
R	Degree of reaction (turbine) [−]
s	Specific entropy [J/kg K]
T	Temperature [K]
$\dot{W}$	Net power output [W]
Z_r	Number of rotor blades [−]

Greek symbols

α	Local heat transfer coefficient
Δ	Difference
ε	Effectiveness [−]
η_{EM}	Electro-mechanical conversion efficiency [−]
η_p	Pump isentropic efficiency []
η_T	Turbine isentropic efficiency (total-to-static) [−]
ν	Velocity ratio (turbine) [−]
ω	Rotational speed (turbine) [rad/s]
ω_s	Specific speed (turbine) [−]

Subscripts

1−11	Rankine cycle state points, see Fig. 2
c	Cold fluid
cond	Condenser
d	Design
h	Hot fluid
HX	Heat exchanger
recup	Recuperator
sink	Heat sink
src	Heat source
spec	Specification
wf	Working fluid

Abbreviations

HTF	Heat transfer fluid
HX	Heat exchanger
PCHE	Printed circuit heat exchanger
PPTD	Pinch point temperature difference
RIT	Radial inflow turbine
VIGV	Variable inlet guide vane
VRS	Variable rotational speed

design already exists can be increased by adopting a more flexible control approach. Indeed, Quoilin et al. [13] demonstrated that a control strategy allowing the evaporating pressure to vary yield better part-load performance compared to the control strategy with this pressure fixed to its value at the design point. In addition, Schuster et al. [14] demonstrated a significant performance improvement potential by equipping the turbine with movable nozzle blades. Finally, Dong et al. [15] demonstrated that the Rankine cycle performance can be improvement by regulating the rotational speed of the expander.

Among the different available expander architectures, the Radial Inflow Turbine (RIT) is particularly promising thanks to its high compactness and its capability to accommodate a large pressure ratio in a single stage [16]. In addition, the commercially available option of equipping the RIT with movable nozzle blades [17,18], also known as variable inlet guide vanes (VIGV), enables efficient off-design operation [17].

To account for off-design performance of the Rankine cycle during the design phase and to consider various control approaches, it is necessary to apply accurate models. In this context the RIT model is of key importance because its efficiency and mass flow rate are strongly affected by operating conditions such as the pressure ratio, and by control variables such as nozzle throat opening and turbine rotational speed [19,20]. Hagen et al. [21] recently proposed two equation-oriented methods for generating the preliminary design and predict the off-design performance of a RIT using a mean-line flow model. This paper proposes similar equation-oriented methods that govern Rankine cycles using a RIT and can be regarded as an extension of Hagen et al. [21].

A selection of methods for analyzing Rankine cycles using a RIT from the open literature is shown in Table 1 (design) and in Table 2 (off-design).

Most of the design methods summarized in Table 1 involves the use of a mean-line RIT model and is formulated as an optimization problem which is solved by a direct search optimization algorithm. A notable exception is the work by Palagi et al. [24] who trained several surrogate models on the basis of a mean-line RIT model and pinch point analysis, and solved the resulting optimization problem by a gradient-based optimization algorithm. Moreover, they demonstrated that the computational cost of their method was two orders of magnitudes lower than the method of using a direct search algorithm to solve the design problem on the basis of Rankine cycle model they used to train their surrogate models [24].

Table 1
Selection of methods for designing Rankine cycles using a RIT in the open literature.

Reference	RIT model	HX model	Optimization algorithm[a]
Hu et al. [22]	Mean-line	Plate HX	Direct
Zhai et al. [23]	Mean-line	Thermodynamic	Direct
Palagi et al. [24]	(Mean-line)	(Thermodynamic)	Gradient (Direct)
Du et al. [25]	Mean-line	Plate HX	Direct
Song et al. [26]	Mean-line	Shell and tube	Not reported
Yao and Zou [27]	Mean-line	PCHE	Not applicable
Li et al. [28]	Mean-line	Thermodynamic	Direct
Present work	Mean-line	Generic	Gradient

[a] The type of optimization algorithm used (direct search or gradient based).

None of the design methods summarized in Table 1 considered the design of heat exchangers (HXs) as a part of the design optimization. Refs. [22−26] assumed for instance predefined pinch point temperature differences (PPTDs) in the HXs. However, some of the design methods applied technology specific models to design the HXs a posteriori. For example, Yao and Zou [27] designed the HXs and the RIT on the basis of predefined cycle state points and effectiveness of the recuperators.

The Rankine cycle performance prediction methods summarized in Table 2 differ in the level of detail and in the in the approach for controlling the cycle. Walnum et al. [29] disregarded the turbine

Table 2
Selection of methods for off-design performance prediction of Rankine cycles using RIT in the open literature.

Reference		RIT model	HX model	Control variables
Walnum et al. (2013)	[29]	Constant efficiency	Compact HXs and Plate HX	p_4 and o_n
Hu et al. (2015)	[22]	Surrogate	Surrogate	p_4
Du et al. (2019)	[25]	Mean-line	Plate HX	p_4 and/or o_n
Schuster et al. (2020)	[14]	Mean-line	Not considered	o_n
This work		Mean-line	Generic	p_4 and any of o_n, ω

performance prediction by assuming a constant RIT efficiency and by allowing the working fluid mass flow rate and the pressure ratio to vary independently of each other. However, they indicated that their simplifications were acceptable due to the VIGV assumption and the moderate variation of the turbine operating conditions. Hu et al. [22] considered a sliding pressure control approach and applied surrogate models for the HXs and the RIT that was generated using a plate HX and a mean-line model, respectively. Schuster et al. [14] considered a constant pressure control approach and disregarded the HX performance prediction by predefining the turbine inlet temperature and the working fluid mass flow rate.

Du et al. [25] documents the most flexible Rankine cycle performance prediction method found in the literature search. They predicted the performance of a Kalina cycle using a RIT with VIGV considering three control approaches: The constant pressure, the sliding pressure and the *optimal* control approach where both the turbine inlet pressure and the nozzle throat opening were optimized simultaneously. Their results show that their *optimal* control approach yield a net power output improvement of up to 11% and 3% compared to the constant pressure and the sliding pressure control approach, respectively. However, they did not consider any control approaches involving variable rotational speed.

Considering the limitations of the methods surveyed in Tables 1 and 2, the aim of this paper is to present and demonstrate two methods for optimizing the design and the performance of Rankine cycles using RIT. The methods proposed in this work are based on a mean-line flow model of the RIT and a generic HX model and consist of the following novel aspects.

(1) The design optimization method optimizes the geometry of the RIT and the HXs, and the Rankine cycle state points simultaneously to maximize the design performance
(2) The performance optimization method allows any combination of the RIT control variables, (nozzle throat opening and rotational speed), to be optimized.
(3) Each of the methods follows an equation-oriented approach and involves the solution of a single mathematical problem that is solved by an efficient gradient-based optimization algorithm.

This paper is organized as follows. The HX- and RIT models, and the problem formulations for the design- and performance optimization methods are described in Sec. 2. The capabilities of the methods are demonstrated in Sec. 3 through a case study for power production from a time variable industrial surplus heat source. First the design optimization method is applied to design the HXs and the RIT of three different Rankine cycles. Thereafter the performance optimization method is applied to predict the annual electricity production from the Rankine cycles considering four different control approaches. The conclusions drawn from this study are summarized in Sec. 4.

2. Methodology

The proposed methods for Rankine cycle design optimization and performance optimization consist of a problem formulation, a Rankine cycle model, and a gradient-based optimization algorithm. The illustration of the methods shown in Fig. 1 is valid for both design optimization and performance optimization.

2.1. The generic heat exchanger model

The present work adopted the generic HX (GHX) model that was introduced in Hagen et al. [30] for estimating HX size and fluid pressure drop. This model does not rely on a certain HX technology. Instead, the GHX model supports any two-fluid HX with a co-current of counter-current flow orientation. Moreover, it accounts for the geometry parameters that are used by the heat transfer coefficient- and pressure gradient correlations. The thermal-hydraulic correlations indicated in Table 3 were developed for channel flow and used to predict the local heat transfer coefficients and the pressure gradients in the HXs. Hence, the cross-sectional geometry of the HXs in this work can defined by the hydraulic diameter, D_h, and the cross-sectional flow area, A_c, for the channels of the hot and the cold fluid.

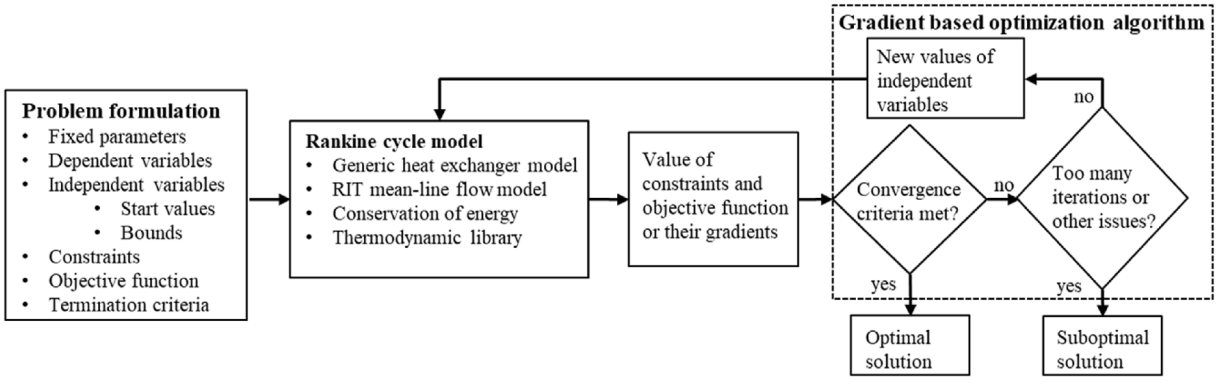

Fig. 1. Overview of the methods for Rankine cycle design- and performance optimization.

Table 3
Thermal-hydraulic correlations applied in this work.

	Heat transfer coefficient	Pressure gradient
Single phase	Gnielinski [31]	Selander [32]
Condensation	Shah [33]	Friedel [34]

The GHX model contain three ordinary differential equations (ODEs) describing heat transfer and fluid flow in a HX. The first ODE describes the relationship between the local heat transfer rate and the temperature difference between the two fluids:

$$\frac{dQ}{dx} = \frac{T_h - T_c}{R} \tag{1}$$

The thermal resistance between the two fluids accounts for convective heat transfer between the fluids and the HX wall, see Eq. (2).

$$R = \frac{1}{P_h \alpha_h} + \frac{1}{P_c \alpha_c} \tag{2}$$

The two remaining ODEs describe the change in pressure per unit length. The ± sign in Eq. (3) is required when integrating through a HX with a counter-current flow orientation: The pressure *decreases* when integrating along the flow direction, but *increases* when integrating against the flow direction.

$$\frac{dp}{dx} = \pm \left(\frac{dp}{dl}\right)_{corr} \tag{3}$$

The analytical solution to Eq. (1), commonly referred to as the LMTD method or the Effectiveness-NTU method, are commonly used but relies on the assumption of constant fluid properties [35]. The GHX model accounts for the variable fluid properties by solving Eqs. (1)) and (3) numerically as an *initial value* problem. This requires that both thermodynamic states at one end of the HX and a stop criterion are defined but enables a once-through calculation procedure.

In contrast to Hagen et al. [30] who used the HX length, L, as the stop criterion, this work introduces the fixed duty stop criterion. This reduces the complexity of the design optimization formulation compared to the formulation in Hagen et al. [30], because consistent duties can be assigned to the GHX model and the problem formulation contain no independent variables for the HX lengths, see Sec. 2.2.

The solution procedure of the GHX model starts at the end of the HX where the thermodynamic states of both fluids are defined ($x = 0$) by using the fourth order Runge-Kutta method to move a step Δx towards the other end (in the x-direction). The outcome of this step is the heat transfer rate and the pressure changes Δp_c, Δp_h that occurs over the interval $[0, \Delta x]$. After that the solution procedure moves step-by-step, as described above, until the accumulated heat transfer rate *exceeds* the predefined duty. At this point the length of the last step is reduced by 10 successive substitutions to ensure a consistent HX duty.

The output of the HX model that is processed to the Rankine cycle model is the heat transfer surface area (Eq. (4)) and the pressure drop of the two fluids.

$$A_s = (P_h + P_c)L \tag{4}$$

2.2. The Rankine cycle design optimization method

The design optimization method generates the preliminary design of a simple recuperated Rankine cycle, see Fig. 2, that maximizes the thermodynamic performance at the design point. The independent variables, constraints and objective function for the Rankine cycle design optimization are shown in Table 4.

The objective of the optimization is to maximize the net power output, see Eq. (16). This objective function was chosen, instead of an economic one, due to the absence of a generic HX cost model. Instead, the cost of an optimized system can be estimated once the HX technology and the Rankine cycle application is determined. However, constraint(s) must be imposed to avoid oversized HXs. In contrast to the commonly used approach of predefining the PPTDs, see Refs. [22–26], the total HX surface area constraint guaranties that the available HX surface area are distributed optimally among the HXs.

The independent variables govern the cycle state points, component efficiencies and design parameters for the HXs and the turbine. One independent variable (the cross-sectional flow area) is introduced for each HX. These variables enable the optimal compromise between pressure drop and overall heat transfer coefficient in the HXs to be found [30]. The inclusion of turbine variables ensures a that the turbine is designed for maximum efficiency at the design point. These 12 variables govern both engineering decision variables such as specific speed and velocity ratio and parameters that are unknown a priori such as the relative velocity and the entropy at the outlet of the nozzle and the rotor. A complete list of the RIT design variables can be found in Hagen et al. [21].

All independent variables are constrained between an upper and a lower bound. Generally, the values of these bounds should be selected such that the optimal solution is not excluded by the bounds, or to avoid unphysical solutions, (e.g. entropy cannot decrease within turbomachinery) and unfeasible solutions. The bounds on the pressure variables may for instance be set to avoid too large internal pressures in the system or to avoid vacuum pressures. In addition, a non-recuperated Rankine cycle can be analyzed by allowing the recuperator effectiveness to be zero.

The Rankine cycle calculation procedure starts by computing the state-points of the cycle, see Fig. 2. These state points are defined by pressure and specific enthalpy and once both properties are known the remaining thermophysical properties are computed by the thermodynamic framework. In this work the thermodynamic calculations were performed using REFPROP v10.0 [36]. The calculation procedure starts by computing the pump inlet state as saturated liquid. This enables the calculation of the pump outlet enthalpy using a prescribed pump efficiency and the independent variable for pump outlet pressure, Eq. (5).

$$h_2 = h_1 + [h(p_2, s_1) - h_1] \,/\, \eta_p \tag{5}$$

Thereafter the turbine outlet enthalpy is computed using the turbine operating conditions and efficiency defined by the independent variables, Eq. (6).

$$h_{5'} = h_5 = h_4 + [h(p_5, s_4) - h_4]\eta_T \tag{6}$$

Now, the maximum enthalpy change that can occur in the recuperator is computed as the enthalpy reduction that would occur if the turbine outlet were cooled down to the temperature of the pump outlet without pressure loss, Eq. (7).

$$\Delta h_{recup,max} = h_5 - h(p_5, T_2) \tag{7}$$

This enables the calculation of the enthalpy change in the recuperator using the recuperator effectiveness, Eq. (8).

$$\Delta h_{recup} = \varepsilon_{recup} \Delta h_{recup,max} \tag{8}$$

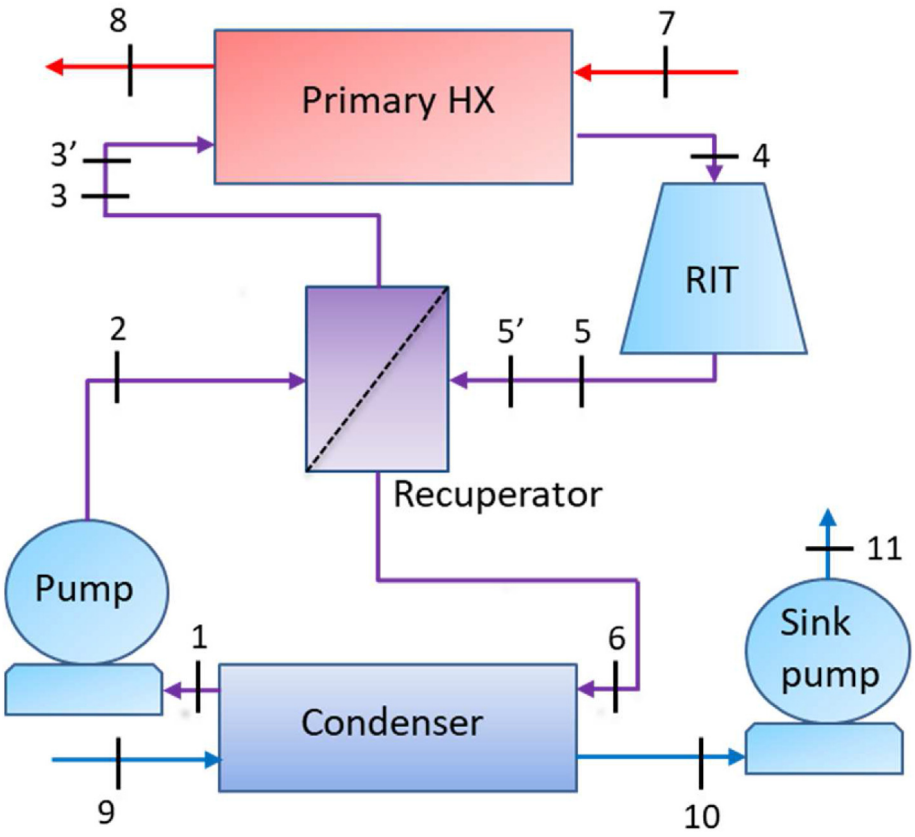

Fig. 2. Illustration of the simple recuperated Rankine cycle analyzed in this work.

Table 4
Independent variables, constraints, and objective function for Rankine cycle optimization.

Description	Symbol/formula	Design optimization	Performance optimization
Independent variables			
Pump inlet pressure	p_1	X	X
Pump outlet pressure	p_2	X	X
RIT inlet pressure	p_4	X	X
RIT inlet enthalpy	h_4	X	X
RIT outlet pressure	p_5	X	X
Heat source outlet temperature[a]	T_8	X	X
Recuperator effectiveness	ϵ_{recup}	X	X
RIT efficiency	η_T	X	X
Number of additional RIT variables		12	7
RIT rotational speed[b]	ω/ω_d		X
RIT nozzle throat opening[c]	$o_n/o_{n,d}$		X
Cross-sectional flow area[d]	A_c	X	
Constraints			
Consistent Primary HX inlet pressure	$p_3 = p_{3'}$	X	X
Consistent RIT outlet pressure	$p_5 = p_{5'}$	X	X
Consistent RIT efficiency	$\eta_T = \eta_{T,calc}$	X	X
Consistent HX length[e]	$L_{HX,calc} = L_{HX}$		X
Number of RIT equality constraints		6	8
Maximum total HX surface area	$\sum_{HX} A_{s,\,HX} \leq A_{s,\,spec}$	X	
Minimum degree of reaction - turbine	$R \geq 0.45$	X	
Objective function			
Maximize net power output, Eq. (16)	$\dot{W}$	X	X

[a] Optional – in this work fixed to the requirements of the heat recovery system.
[b] Optional – in this work applied for the VRS and "VRS and VIGV" control approaches.
[c] Optional – in this work applied for the VIGV and "VRS and VIGV" control approaches.
[d] Three variables – one for each HX – each variable represents flow area for both fluids.
[e] Three constraints – one for each HX.

Then, the inlet enthalpy of the Primary HX and the condenser can be computed by Eqs. (9)-(10).

$$h_{3'} = h_3 = h_2 + \Delta h_{recup} \tag{9}$$

$$h_6 = h_5 - \Delta h_{recup} \tag{10}$$

The mass flow rates of the working fluid and heat sink can now be calculated by conservation of energy assuming that the HXs are thermally isolated from the ambient, Eqs. (11)-(12).

$$\dot{m}_{wf} = \frac{h_7 - h_8}{h_4 - h_3}\dot{m}_{src} \tag{11}$$

$$\dot{m}_{sink} = \frac{h_6 - h_1}{h_{10} - h_9}\dot{m}_{wf} \tag{12}$$

Now, the duty and the thermodynamic states at one end of each HX are defined enabling solving the HXs. More specifically, the Primary HX is solved from the hot to the cold end, and the recuperator and condenser are solved from the cold to the hot end using the GHX model described in Sec. 2.1. The outcome of the GHX model that are processed further is the pressures p_3, p_4, p_7, and p_{12} and the size (length and surface area) of each HX.

The RIT performance was accounted for by using the mean-line flow model documented in Hagen et al. [21] This model assumes that the flow is *uniform* along the blade span, predicts the isentropic efficiency on the basis of an *empirical loss model* and has been *validated* against experimental data [21]. The RIT model starts by computing the isentropic enthalpy change, $\Delta h_{is} = h_5 - h(p_6, s_5)$ and the spouting velocity $C_0 = (2\Delta h_{is})^{0.5}$ using the RIT inlet state and outlet pressure defined by the independent variables. This enables the calculation of the rotational velocity and the rotor radius using the independent RIT variables for specific speed and velocity ratio by Eqs. (13)-(14)

$$\omega = \frac{(\Delta h_{is})^{0.75}}{\left(\dot{m}_{wf}/\rho_5\right)^{0.5}}\omega_s \tag{13}$$

$$r_4 = \frac{C_0}{\omega}\nu \tag{14}$$

Thereafter the independent RIT geometry variables are used to generate the RIT geometry. The geometry parameters involved in the mean-line model are illustrated in Fig. 3 and the reader is referred to Hagen et al. [21] for further details on how their values are determined.

Thereafter the velocity triangles, the thermophysical properties and the losses in the RIT are computed using conservation equations, the remaining independent RIT variables and the empirical loss model (Eq. (1-18) in Hagen et al. [21]).

The sink pump increases the pressure of the heat sink fluid by a magnitude equal to the condenser heat sink pressure drop. More specifically, $p_{13} = p_{11}$ and the sink pump outlet enthalpy is computed by Eq. (15).

$$h_{11} = h_{10} + [h(p_{11}, s_{10}) - h_{10}] / \eta_p \tag{15}$$

The Rankine cycle calculation procedure ends by computing the net power output as the difference between the produced power and the power consumed by the pump motors accounting for the electro-mechanical conversions, Eq. (16).

$$\dot{W} = \dot{m}_{wf}(h_4 - h_5)\eta_{EM} - \dot{m}_{wf}(h_2 - h_1)/\eta_{EM} - \dot{m}_{sink}(h_{11} - h_{10})/\eta_{EM} \tag{16}$$

The design optimization method takes advantage of equality constraints to ensure that the Rankine cycle model is consistent. For instance, two equality constraints are imposed to ensure that $p_3 = p_{3'}$ and that $p_5 = p_{5'}$. In addition, an equality constraint is imposed to ensure that the value of the RIT efficiency variable equals the predicted value of the RIT model. The RIT equality constraints consists of the following: three constraints to ensure that

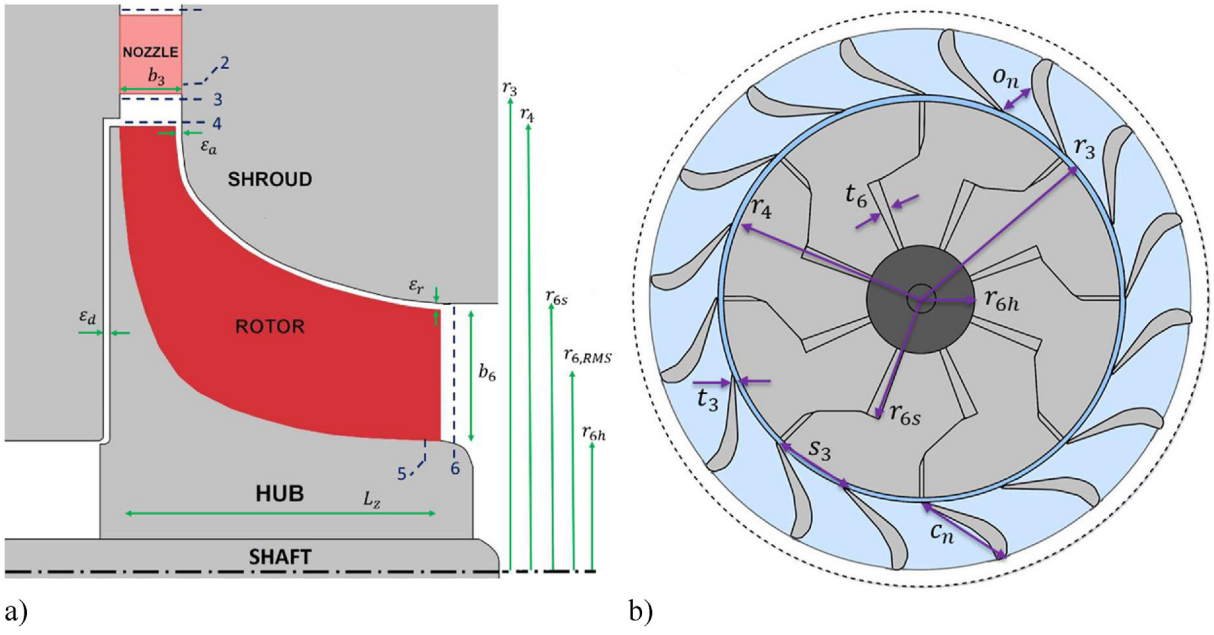

Fig. 3. Illustration of the RIT, and the geometry and state-points involved in the RIT mean-line model.

the mass flow rate is conserved and that its value equals the working fluid flow rate computed by Eq. (11), two constraints to ensure that the entropy distribution defined by the independent variables are consistent with the predicted losses in the nozzle and the rotor, and one constraint to ensure that the rotor outlet pressure computed by the RIT model equals p_5. The reader is referred to Hagen et al. [21] for the equations used to compute the RIT equality constraints.

In addition, other equality- or inequality constraints may readily be imposed to ensure that the optimization result satisfies additional design requirements such as dry expansion. In this work an inequality constraint was imposed to ensure a certain turbine degree of reaction. This constraint was proposed by Aungier [37] and applied by Hagen et al. [21].

The gradient-based optimization algorithm applied in this work was NLPQL [38]. This is a sequential quadratic programming (SQP) method that can be applied for solving both constrained optimization problems and systems of nonlinear equations. Gradients are calculated using a second order central difference approximation for numerical differentiation. The Kerush Kuhn Tucker (KKT) optimal criterion is set to 1.0E-4 and the maximum number of iterations is set to 100. This means that NLPQL returns an infeasible or suboptimal solution if the KKT optimal criterion is not met within 100 iterations or other issues occur [38], see Fig. 1. This means that the iterative procedure indicated in Fig. 1 repeats itself 100 times unless the KKT optimally criterion is met or other issues occur.

2.3. The Rankine cycle performance optimization method

The Rankine cycle performance optimization method maximizes the performance of a Rankine cycle whose design exists at a given operating condition (design or off-design). The independent variables, constraints and objective function for the Rankine cycle performance optimization method are shown in Table 4.

The performance optimization method has several similarities with the design optimization method. First it applies the same gradient-based optimization algorithm. Moreover, both methods have the similar set of independent variables and equality constraints related to cycle state points and component efficiencies, see Table 4, and their calculation procedures of the cycle (Eq. (5)-(12)) and HXs are identical. The main difference between the methods is that there are no independent component geometry variables in the performance optimization method. Instead, the geometry of the HXs and the RIT are solely defined by the fixed parameters. Furthermore, the novel treatment of choked flow introduced by Hagen et al. [21] which ensures physical consistent results in the case of supersonic velocities, is adopted in this work. This requires two additional independent variables and equality constraints to increase the resolution of the entropy distribution within the RIT and, in the case of supersonic velocities, an inner iteration to compute the thermodynamic state at the point where the flow velocity exceeds the speed of sound. The reader is referred to Hagen et al. [21] for further details on the performance evaluation of the RIT. Finally, the HX lengths are in the performance optimization method imposed as equality constraint to ensure consistent HX models.

The optional independent variables for turbine rotational speed and nozzle throat opening enable a selection of four approaches for controlling the Rankine cycle. The *sliding pressure* control approach occurs when both the turbine rotational speed and the nozzle throat opening are fixed parameters. This is a common approach for controlling Rankine cycles and involves changing the turbine inlet pressure to balance system parameters such as the working fluid mass flow rate [25]. This is the least flexible control approach considered in this work. Actually, if the heat source outlet temperature T_8, is a fixed parameter, as is the case for the demonstration of the method, see Sec. 3, the number of equality constraints equals the number of independent variables. In this case the mathematical problem is a system of nonlinear equations with a single unique solution. Without an obvious reason for prescribing the heat source outlet temperature, T_8 should be an independent variable resulting in a mathematical problem for sliding pressure control approach with one degree of freedom.

The variable rotational speed (VRS) control approach occurs when the turbine rotational speed is an independent variable while the nozzle throat opening is a fixed parameter. VRS assumes that the turbo-generator system can deliver electric power at the grid frequency despite the variable turbine rotational speed. This can be achieved by using a high-speed generator and a flexible frequency converter system adjusting the frequency of the produced power to the grid frequency [15].

The variable inlet guide vane (VIGV) control approach occurs when the nozzle throat opening is an independent variable and the turbine rotational speed is a fixed parameter. VIGV assumes that the RIT is equipped with movable nozzle guide vanes that modifies the nozzle throat opening by rotating around a pivot point [17,18].

In the fourth control approach, in this work referred to as “VRS and VIGV”, both the nozzle throat opening, and the rotational speed are independent variables.

2.4. Discussion of the problem formulations

Developing effective methods for designing and analyzing Rankine cycles accounting for the physics within its main components is a challenging task that requires creativity and a solid understanding of the mathematical models involved. We believe the proposed methods for Rankine cycle design- and performance optimization have some advantages and contain some novelties that are worth highlighting.

- The proposed methods account for the thermophysical properties of the involved fluids by means of general heat transfer and pressure gradient correlations in the HXs and a loss model within the RIT model. One advantage of using general models based on physics is the confidence of obtaining results of reasonable accuracy for a broad range of conditions. Consequently, we regard the proposed methods applicable to design and analyze Rankine cycles for various applications (e.g. different heat sources and HX technologies) and with any fluid available in the thermodynamic library as a potential working fluid candidate. Moreover, the same underlying HX- and RIT model are applied for both the design- and the performance optimization method yielding a smooth transition between the two methods.
- The proposed methods avoids the need for defining the flow rates of the working fluid and the heat sink. Indeed, they are computed using HX energy balance, see Eqs. (11)-(12). We believe this simplifies the process of obtaining reasonable start values of the independent variables, and of adjusting them to different working fluids or heat source characteristics.
- In contrast with the published design methods in Table 1, with the notable exception of the surrogate model approach in Ref. [24], the proposed design optimization method avoids the use of inner iteration(s) to compute the Rankine cycle performance. Indeed, all the equations involved requires only explicit

computations (inner iterations are limited to thermodynamic function calls) and inner iteration loops are replaced by equality constraints that are handled by the optimization algorithm. Consequently, the Rankine cycle model doesn't have to be solved at each intermediate optimization iteration and an efficient gradient-based algorithm can be applied, leading to a reduction in the computational cost [39].

3. Case study

Energy-intensive industry release large amounts heat that can be utilized for power production. Germany industry for instance, releases more than 200 TWh every year to the environment and the annual electricity production potential from the steel, glass and cement industry alone using Rankine cycles are several TWh_e [40]. This section demonstrates the capabilities of the proposed methods through the design and performance prediction of Rankine cycles utilizing industrial surplus heat. The industrial facility is a representative Norwegian ferroalloy plant with an annual ferrosilicon production of 100 000 ton and we considered heat recovery from batch-wise metal casting. Each "batch" consists of an amount of liquid metal that is distributed into multiple molds in which it solidifies and cools down to ambient temperature. The latent and sensible heat that is released in this process is significant but seldom utilized [41]. However, a concept for capturing and utilizing this heat is proposed, see Ref. [42]. This heat recovery system consists of a cooling tunnel in which heat from the molds is transferred to a heat transfer fluid (HTF), thermal energy storage to smooth temperature variations, and a Rankine cycle as illustrated in Fig. 4.

The time dependent HTF characteristics for a 1-h period, see Fig. 5, were generated by means of the dynamic model of the heat recovery system described in Ref. [42]. In the first half an hour, molds containing liquid metal enter the cooling tunnel one by one as illustrated by the stepwise increase in the HTF temperatures and the Primary HX duty. In the second half an hour there is no further heat input to the cooling tunnel and the heat delivered to the Rankine cycle is mainly provided by the thermal energy storage, illustrated by the constantly decreasing HTF temperatures. The heat recovery system operates at a cyclic-steady state which means that the process depicted in Fig. 5 repeats itself every hour.

3.1. Setup for the design optimizations

The present case study focuses on the Rankine cycle by considering the HTF characteristics as fixed parameters. Furthermore, the proposed methods rely on the RIT as the expander technology and the Rankine cycle layout depicted in Fig. 2. Consequently, this section governs the selection of working fluid, HX technology and the remaining fixed parameters used for the design optimizations. The fixed parameters used for the present case study are shown in Table 5. The relatively low heat sink inlet temperature can be justified by the Norwegian climate. As the working fluid selection based on quantitative analysis is out of the scope of this article and the HTF temperature exceeds 500 °C we want to highlight a couple of advantages of our selected working fluid for the present case study: First, in contrast to most organic fluids whose thermal stability when their temperature exceeds 300−350 °C could be questioned, CO_2 is stable at least up to 600 °C [43]. Secondly, the moderate working fluid pressure ratio of CO_2 power cycles is ideal for applying a single stage RIT. Indeed the single stage RIT is regarded as the most suitable expander technology for CO_2 power cycles of a few MW_e [44].

Compact HXs such as PCHE, Plate fin or other HXs with micro tubes have been suggested for CO_2 Rankine cycles due to their high operating pressure [45]. For this reason, a low value for the hydraulic diameter was used such that the GHX model represented a generic compact HX. The value for D_h in Table 5 was used for the channels of both the hot and cold fluid in all HXs. Thus, the perimeter, or the heat transfer surface area per unit length of each channel in each HX were computed by Eq. (17) where A_c is an independent variable, see Table 4.

$$P_c = P_h = \frac{4A_c}{D_h}. \tag{17}$$

A theoretical study that accounted for the turbomachinery design demonstrated that the working fluid pressure that maximized the thermodynamic performance of a CO_2 Rankine cycle to

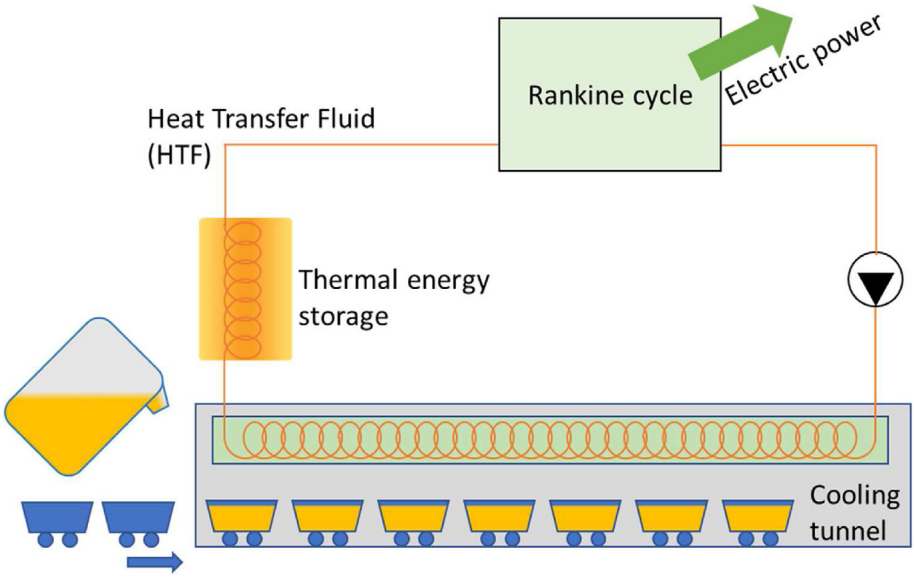

Fig. 4. Concept diagram of the heat recovery system.

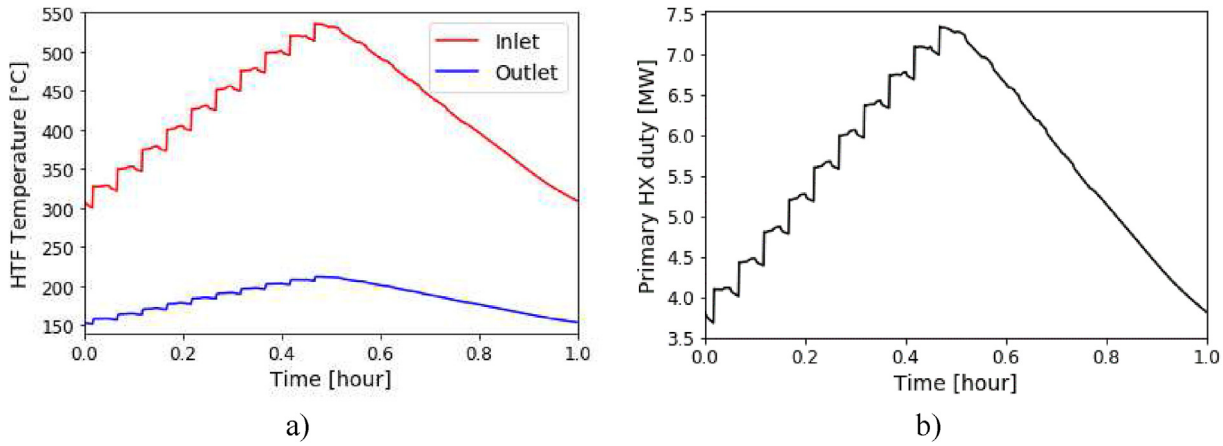

Fig. 5. Time-dependent characteristics of the Rankine cycle heat source.

Table 5
Fixed parameters of the Rankine cycle.

HTF medium	CO_2
HTF mass flow rate	18.2 kg/s
HTF pressure, p_7	200 bar
Heat sink medium	Water
Heat sink inlet temperature, T_9	10 °C
Heat sink outlet temperature, T_{10}	20 °C
Working fluid medium	CO_2
Maximum working fluid pressure, upper bound for p_2	200 bar[a]
HX hydraulic diameter, D_{hyd}	1.2 mm
Total HX surface area, $A_{s,\,spec}$	500 m^2[b]
Pump efficiency, η_p	0.65
Electromechanical efficiency, η_{EM}	0.95

[a] Must be respected at both design and off-design operating conditions.
[b] Only relevant for design optimization.

be up to 400 bar [46]. On the other hand, existing CO_2 Rankine cycle prototypes considers much lower working fluid pressures [10]. Considering this discrepancy, an upper bound was set on the working fluid pressure to avoid proposing something unrealizable, see Table 5. The design optimizations were performed using the problem formulation from Table 4 and the fixed parameters in Table 5. The time dependent characteristics are limited to the HTF temperatures illustrated in Fig. 6.

Three design points were considered. More specifically, one

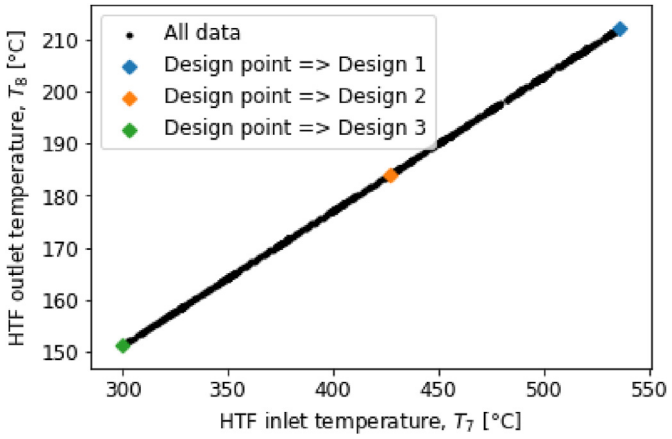

Fig. 6. Scatterplot of the HTF temperatures from Fig. 5(a). The characteristics used for the design optimizations leading to three *designs* are highlighted.

Table 6
Design point HTF characteristics adopted in this work.

Design		1	2	3
HTF inlet temperature, T_7	[°C]	535	427	300
HTF outlet temperature, T_8	[°C]	212	184	152
Primary HX duty	[MW]	7.33	5.61	3.68

design optimization was carried out considering each of the three HTF characteristics indicated with colored markers in Fig. 6 as fixed parameters. The numerical values of the design point HTF temperatures and the resulting Primary HX duties are shown in Table 6.

3.2. Design optimization results

T-s diagrams of the Rankine cycle processes from the design optimizations are shown in Fig. 8. All processes are transcritical because the high pressure exceeds the working fluid critical pressure while the low pressure is below the critical pressure illustrated by the heat rejection to the heat sink occurring within the phase envelope. Moreover, the pinch point of the Primary HX moves from its cold end (Design 1 and 2) to its hot end (Design 3).

Although Design 2 and Design 3 had a lower pump outlet pressure, p_2, than Design 1 this variable reached its upper bound in all cases. This was required to avoid working fluid pressure *exceeding* 200 bar at off-design operating conditions. Indeed, the blue curve in Fig. 12(c) shows that p_2 increases with the HTF temperature for the sliding pressure control approach. The numerical values for p_2 of Design 2–3 shown in Table 7 were found by manually iterating between design optimization and a subsequent off-design performance prediction of the sliding pressure control approach.

The component geometry obtained by the design optimizations are shown in Table 7 (HXs) and Table 8 (RIT). These tables show that the design point HTF characteristics do affect the optimized component geometry. Notably, there is positive correlation between turbine size and the design point Primary HX duty.

One drawback of gradient-based optimization algorithms is that they may converge to a local optimum close to the starting point used for optimization. In addition, the convergency to an optimum is only guaranteed if the involved functions are smooth. The numerical routines within the thermodynamic framework and the successive substitution method within the GHX model might be sources of non-smoothness. To assess the robustness of the proposed design optimization method, we carried out 100

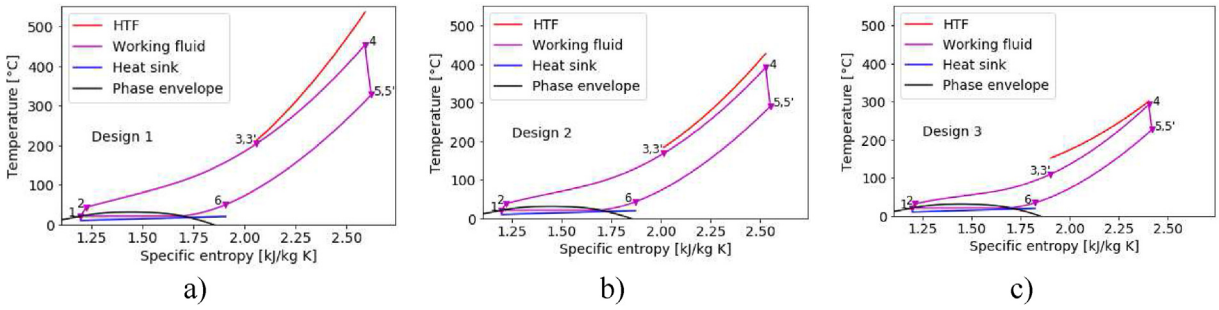

Fig. 7. T-s diagrams of the Rankine cycle processes obtained by the design optimizations.

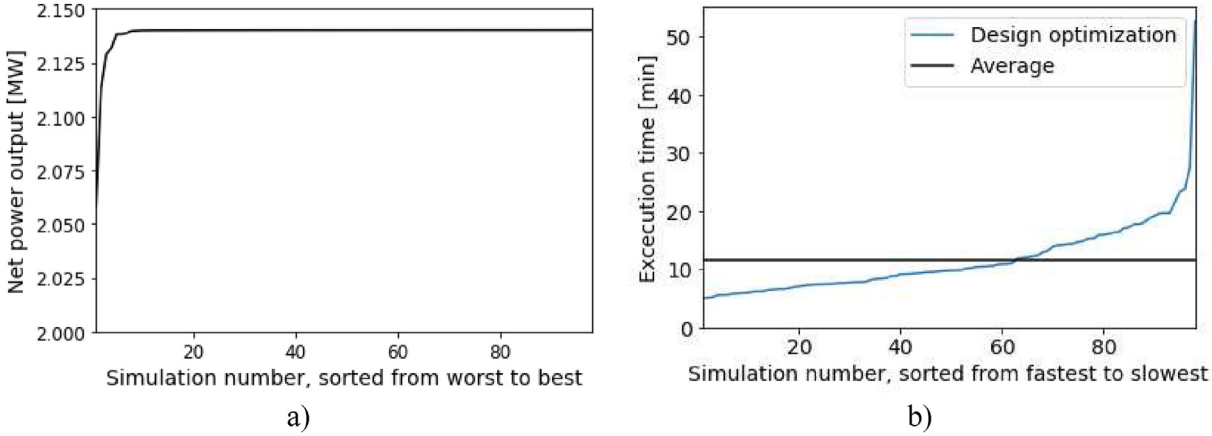

Fig. 8. Objective function value (a) and execution time (b) from 98 of the 100 optimizations of Design 1 that converged to an optimum. The independent variables were assigned random start values in all cases.

Table 7
Selection of numerical results obtained by the Rankine cycle design optimizations.

Design		1	2	3
Pump outlet pressure, p_2	[bar]	200	163	120
Pump inlet pressure, p_1	[bar]	58.3	58.5	58.3
Working fluid mass flow rate	[kg/s]	23.5	20.2	15.9
Net power output	[MW]	2.14	1.41	0.66

Table 8
HX geometry obtained by the Rankine cycle design optimizations.

Design		1	2	3
Primary HX length	[m]	1.59	1.71	1.40
Primary HX cross sectional area	[10^{-3} m^2]	12.5	13.4	15.8
Primary HX surface area	[m^2]	130	150	145
Recuperator length	[m]	1.06	1.09	1.14
Recuperator cross sectional area	[10^{-3} m^2]	23.7	21.8	20.8
Recuperator surface area	[m^2]	164	155	155
Condenser length	[m]	1.04	1.06	1.20
Condenser cross sectional area	[10^{-3} m^2]	30.3	28.2	25.5
Condenser surface area	[m^2]	205	195	200

optimizations of Design 1 using random start values of the independent variables. Only two of these failed to converge to an optimum. This is an indication that the above-mentioned sources of non-smoothness are not a major concern for convergency. The objective function value and the execution time obtained on a personal computer with an Intel Core i7-8650U processor from the remaining optimizations are shown in Fig. 9. As seen in Fig. 9(a),

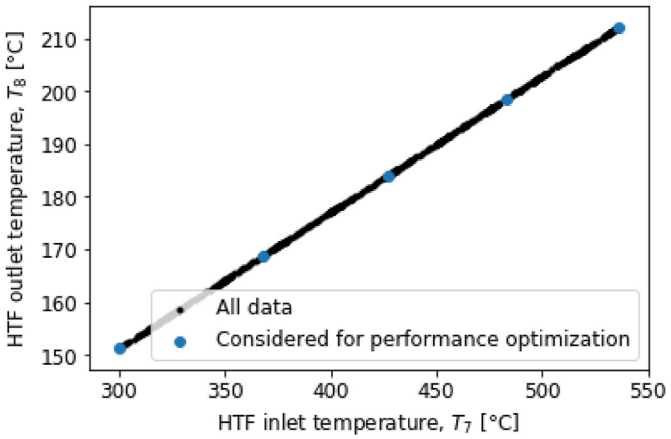

Fig. 9. Scatterplot of the HTF temperatures from Fig. 5(a). The characteristics used for the performance optimizations are highlighted.

most of the optimizations yield almost the same maximized net power output. More specifically, the 88 best optimizations deviate with less than 0.01% in terms of net power output and 2% in terms of optimized values of the independent variables. The consistency in the optimization results is a strong indication that the optimization problem contains few local optimums and that the gradient-based algorithm in most cases converged to the global optimum. The average execution time was 11.5 min and 53% of the simulations spent less than 10 min to converge, see Fig. 9(b).

Table 9
RIT geometry and rotational speed obtained by the Rankine cycle design optimizations.

Design			1	2	3
Nozzle	r_3	[mm]	88.61	84.75	78.81
	b_3	[mm]	3.45	3.69	4.06
	s_3	[−]	28.74	27.30	25.36
	$o_{n,d}$	[mm]	10.26	9.67	8.97
	t_3	[mm]	0.46	0.44	0.40
	c_n	[mm]	38.22	36.31	33.73
Rotor	r_4	[mm]	86.15	82.13	75.94
	r_{6s}	[mm]	60.31	57.49	53.15
	r_{6h}	[mm]	43.25	40.88	36.97
	ω_d	[kRPM]	40.65	37.20	30.88
	b_4	[mm]	3.45	3.69	4.06
	Z_r	[−]	16	17	17
	t_6	[mm]	1.72	1.64	1.52
	A_5	[$(cm)^2$]	19.98	18.58	16.44
	L_z	[mm]	25.59	24.92	24.27
	c_r	[mm]	41.88	40.64	39.84
	ε_a	[mm]	0.40	0.40	0.40
	ε_r	[mm]	0.40	0.40	0.40
	ε_d	[mm]	4.31	4.11	3.80
Rotor visualization (sizes in mm)			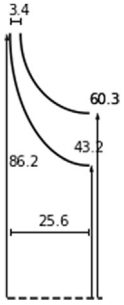	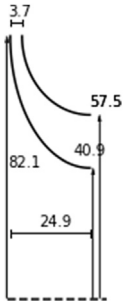	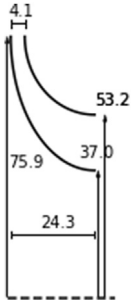

3.3. Setup for the performance optimizations

The performance optimizations were carried out using the independent variables, constraints and the objective function showed in Table 4. In addition, the parameters of Table 5 and the component geometries in Tables 8 and 9 were provided as fixed parameters.

One purpose of the performance optimizations is to estimate the annual electricity production from the Rankine cycles designed in the previous section. To this aim the performance of these Rankine cycles were evaluated at five different HTF characteristics, see Fig. 9. The scatterplot in Fig. 9 shows a perfect linear correlation between the HTF inlet and outlet temperatures. Consequently, the HTF temperatures were defined by the HTF inlet temperature, see Fig. 10–13, because it has only one corresponding HTF outlet temperature. Finally, all four approaches for controlling the Rankine cycle described in Sec 2.3 were considered.

3.4. Performance optimization results

3.4.1. Design 1

The performance optimization results of Design 1 are shown in Fig. 11. Each of the plots (a,b,c,d) govern a certain performance metric, whereas each colored line represents a certain control approach. The result from the corresponding design optimization is highlighted with a black diamond shaped marker.

Fig. 11(a) shows that working fluid mass flow rate is decreasing with decreasing HTF inlet temperature. One option for reducing the turbine mass flow rate is to reduce the pressure ratio across the RIT [21]. Indeed, Fig. 11(b) shows that the maximum working fluid pressure decreases with decreasing HTF inlet temperature for the sliding pressure and the VRS control approach. Alternatively, the mass flow rate may be reduced by reducing the nozzle throat opening [21]. Indeed, the VIGV and "VRS and VIGV" control approaches maintain the maximum working fluid pressure around 200 bar by reducing the nozzle throat opening, see Figs. 11(b) and Fig. 12 (b).

Fig. 11(c) shows that the turbine isentropic efficiency drops dramatically from the design value of 87.3% and down to 55.6% for the *sliding pressure* control approach and that the other control approaches improve the off-design RIT efficiency. Notably the VRS and "VRS and VIGV" control approach improves the RIT efficiency by reducing the rotational speed, see Fig. 12(a).

The net power output is shown in Fig. 11(d). All control approaches yield similar performance at the design point. However, the sliding pressure control approach yield a lower off-design performance than the other control approaches. VRS outperforms the sliding pressure control approach due to the improved RIT isentropic efficiency, while the improvements of the VIGV are mainly due to the higher working fluid pressure.

3.4.2. Design 2

The main results from the performance optimizations of Design 2 are shown in Fig. 13. Similarly, as for Design 1, VIGV and "VRS and VIGV" control approaches facilitate operation with higher working fluid pressure than sliding pressure by reducing the nozzle throat opening, see Fig. 13(b and c). Indeed, the pump outlet pressure of the VIGV control approach went to its upper bound of 200 bar for

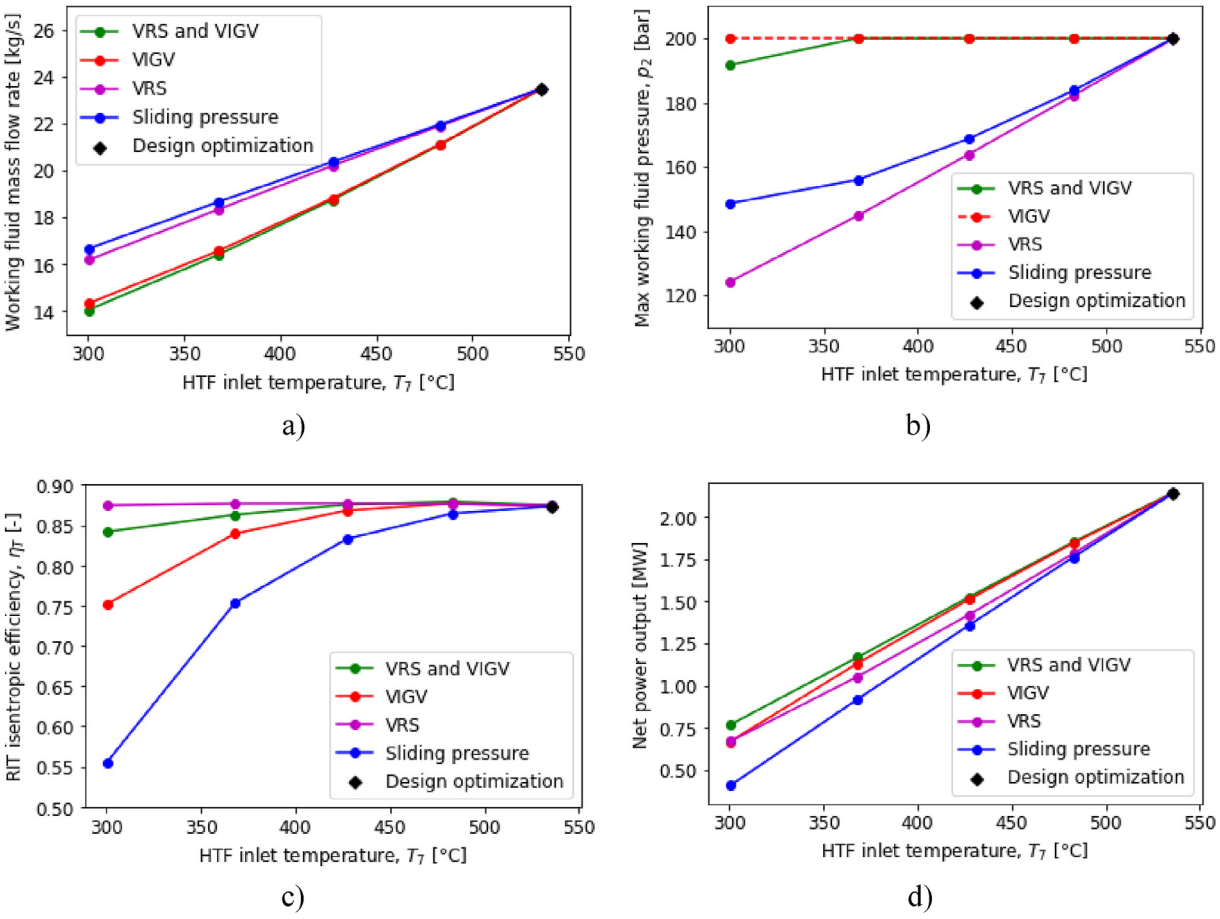

Fig. 10. Performance optimization results of Design 1.

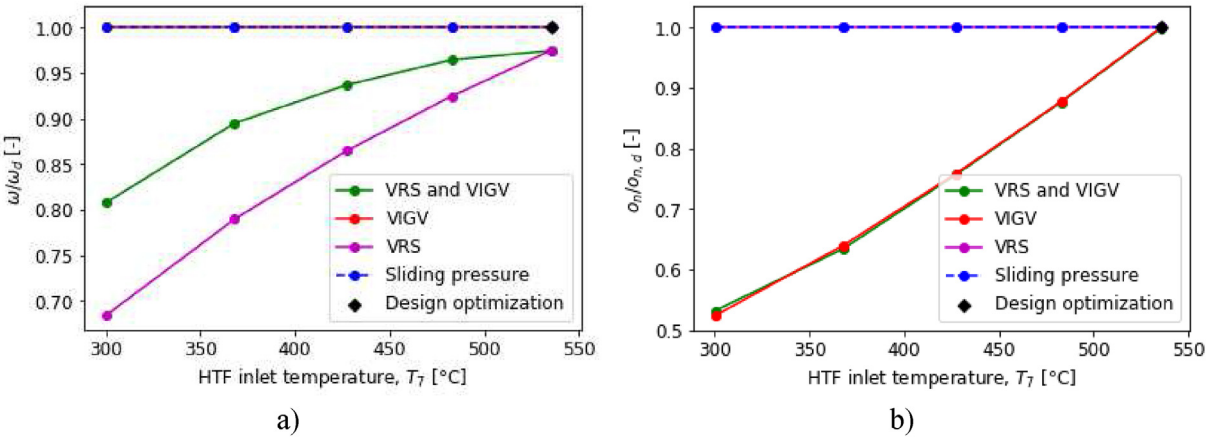

Fig. 11. Optimized values of the RIT control variables obtained from the performance optimizations of Design 1.

all cases. The increased pump outlet pressure is beneficial from the thermodynamic point of view and VIGV outperforms the sliding pressure control approach for such cases which includes the design operating point, see Fig. 13(d).

Fig. 13(a) shows that the RIT efficiency of the sliding pressure control approach are higher than 80% in all cases except for the smallest HFT inlet temperature. Consequently, VRS yield only a slight net power improvement over the sliding pressure control approach, se Fig. 13(d).

3.4.3. Design 3

The main results from the performance optimizations of Design 3 are shown in Fig. 14. Fig. 14(a) shows that the RIT isentropic efficiency drops from the design value of 87.6% and down to 74.3% for

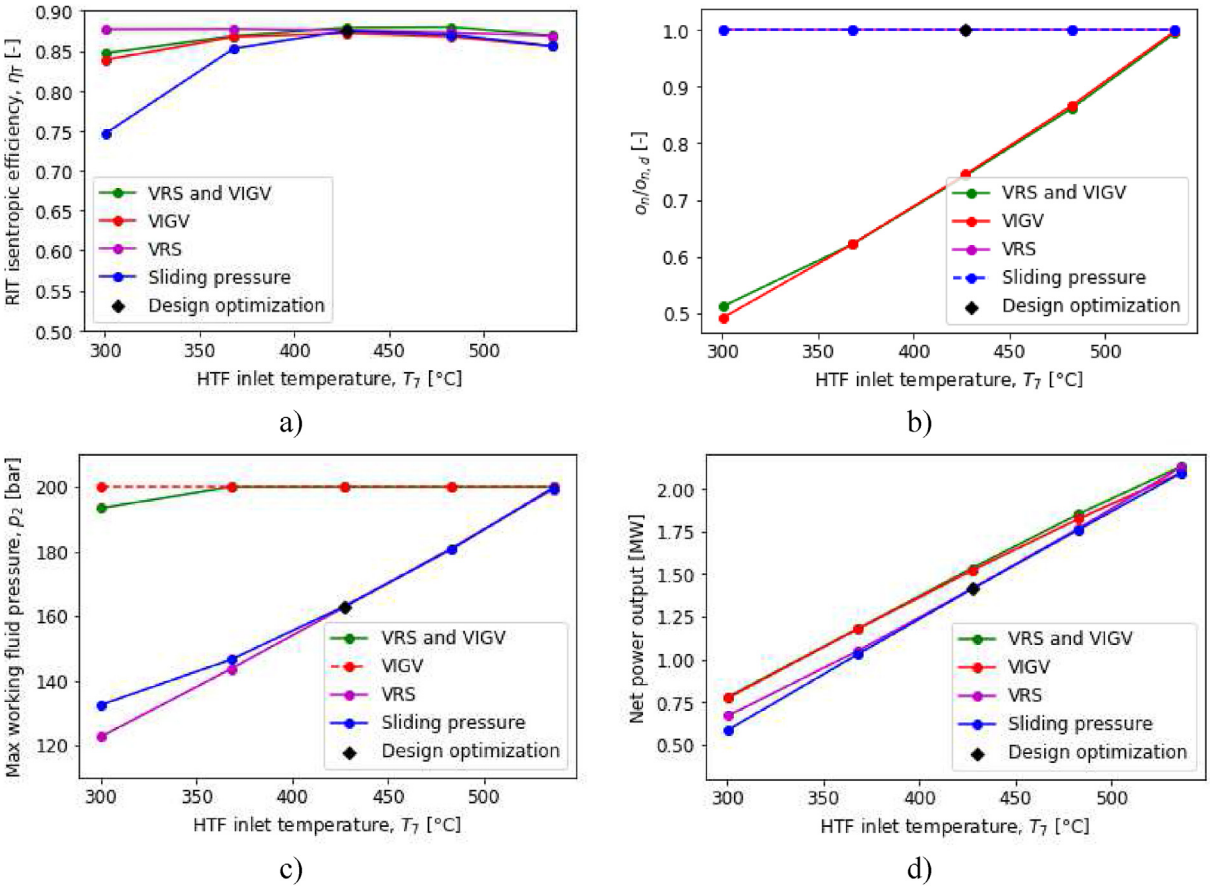

Fig. 12. Performance optimization results of Design 2.

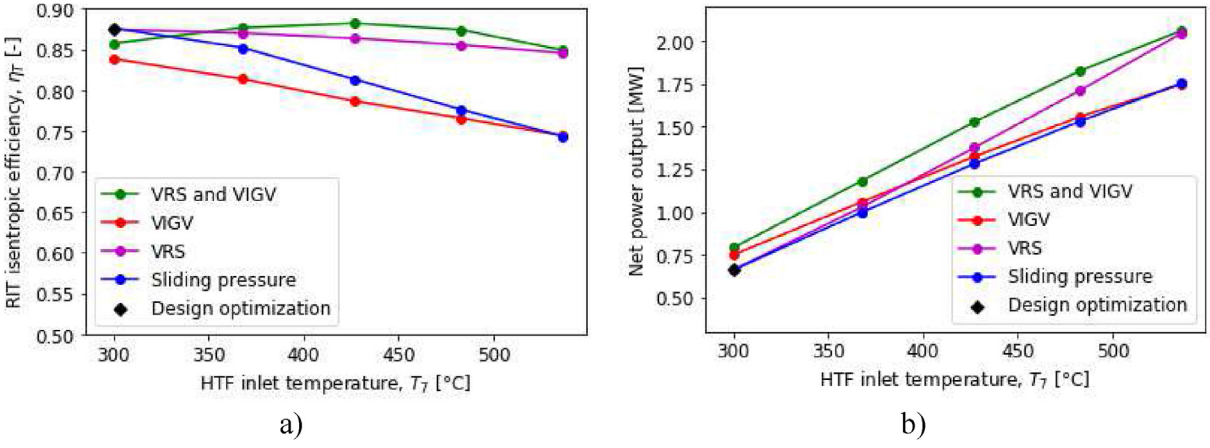

Fig. 13. Performance optimization results of Design 3.

the sliding pressure control approach. In contrast to Design 1, VIGV yields a lower RIT efficiency than the sliding pressure control approach.

The net power output from Design 3 is shown in Fig. 14(b). In this case VIGV yield only a slight performance improvement over the sliding pressure control approach. VRS also improves over the sliding pressure control approach, particularly at the largest HTF temperatures. "VRS and VIGV" maintain a significant net power improvement over sliding pressure control approach for all cases.

3.4.4. *Computational cost*

In order to assess the computational cost of the performance optimization method all performance optimization applied the same set of start values and bounds for most of the independent variables. The only exception is the variable, h_5, whose bounds and start value was tailored accounting for the HTF inlet temperature. The average execution time of the performance optimizations of 3.2 min is less than one third of the average execution of the design optimizations. A possible explanation for this is that the performance optimization method involves fewer independent variables

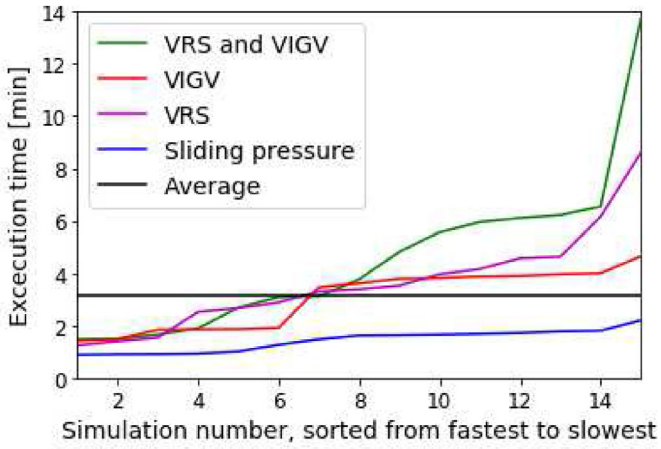

Fig. 14. Execution time of the performance optimizations carried out in this work.

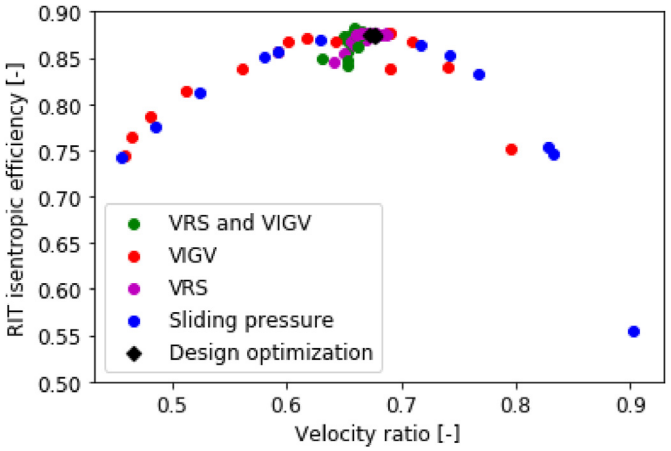

Fig. 16. RIT efficiencies and velocity ratios obtained by the design- and performance optimizations of designs 1–3 in this work.

than the design optimization method. The execution time of the performance optimizations of sliding pressure, the control approach with fewest independent variables, is lower than the execution time of the performance optimizations of the other control approaches, see Fig. 15.

3.5. Discussion of the case study results

The results of the case study are summarized in Fig. 16. The net power output vs. time shown in Fig. 16(a,b,c) were estimated by means of linear interpolations using the HTF inlet temperature vs. time depicted in Fig. 5(a) and the net power output results of Figs. 11(d), 13(d) and 14(b). Thereafter the hourly electricity production were estimated as the area under the curves in Fig. 16(a,b,c) by the trapezoidal method for numerical integration. Finally, the annual electricity production estimates of Fig. 16(d) were computed assuming that the system operates 95% of the year.

Fig. 16(d) show that the "VRS and VIGV" yield the largest annual electricity production among the control approaches for all designs.

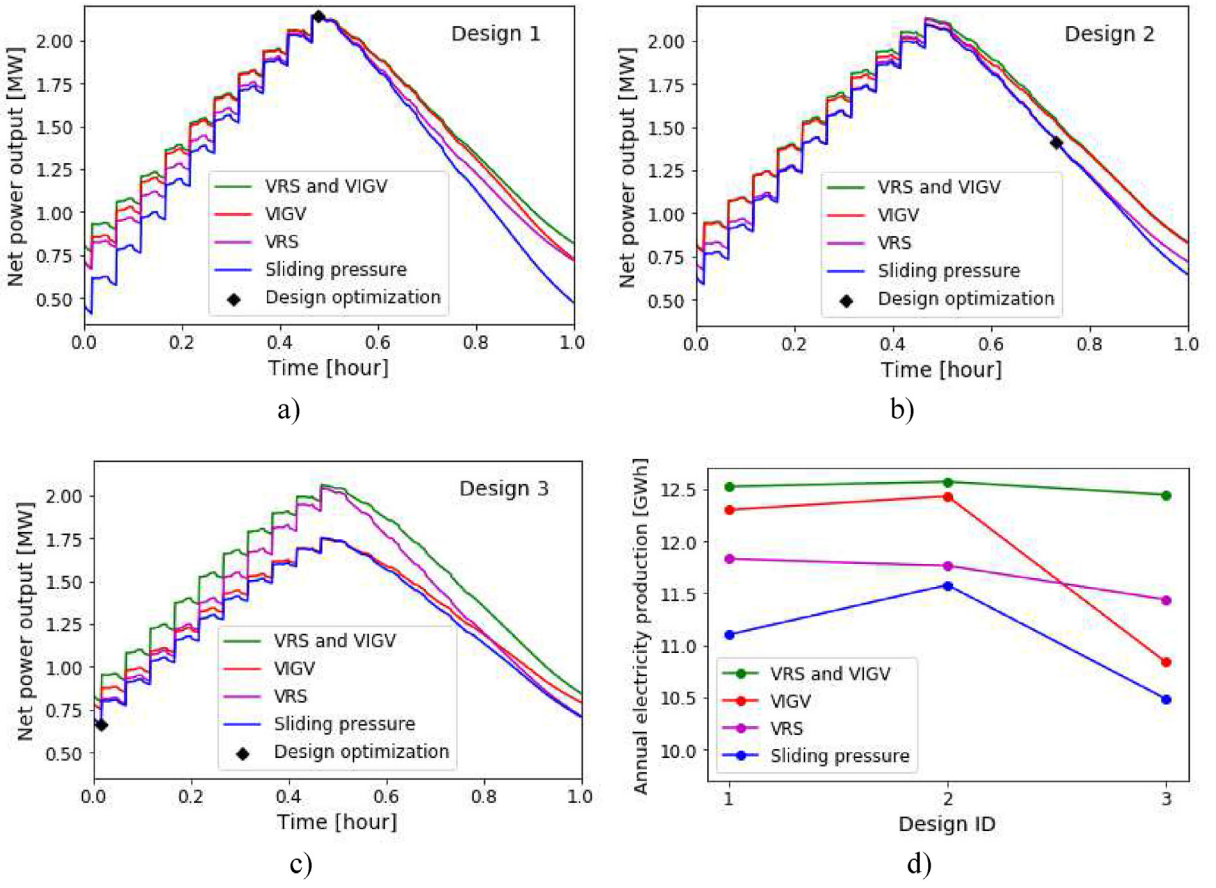

Fig. 15. Net power vs. time computed by linear interpolation for Designs 1–3 (a,b,c) and the resulting annual electricity production (d) from the present case study.

In addition, and in contrast to the other control approaches, "VRS and VIGV" yield similar annual electricity production for the three designs indicating that the flexibility associated with this control approach compensates for the effect of RIT and HX design on the thermodynamic performance of the Rankine cycle.

Sliding pressure yield the lowest annual electricity production among the control approaches for all designs. Notably, the largest electricity production from the sliding pressure control approach occurs for Design 2 where the components were designed for an average operating point, see Fig. 7, thus enabling the Rankine cycle to be operated closer to its design point than the other designs.

VIGV doesn't implicate improved RIT efficiency. Indeed, the results of Figs. 11(c), 13(a) and 14(a) show that VIGV only increase the RIT efficiency over the sliding pressure control approach for cases when the HTF inlet temperature is lower than its value at the design point. This agrees with the results of Du et al. [25] whose optimal control approach only predicted larger RIT efficiency than their sliding pressure control approach for the cases when the heat source quantity was lower than its design value.

One of the key parameters affecting the turbine efficiency is the velocity ratio defined as the ratio between the velocity of the rotor blade tip and the spouting velocity which is proportional to the square root of the isentropic enthalpy drop, see Eq. (14). Indeed, as depicted in Fig. 16 there is a strong correlation between the RIT efficiency and the velocity ratio. The figure also show that the lower RIT efficiencies obtained by the sliding pressure and the VIGV control approaches are caused by the velocity ratio deviating from its design value. On the other hand, the VRS and "VRS and VIGV" control approaches optimized the rotational speed such that velocity ratio and the RIT efficiency are close to their values at the design point.

4. Conclusions

This paper presented a method for optimizing the design of Rankine cycles using RIT. A novelty of this method is that the geometry of the HXs and the RIT is optimized simultaneously with the cycle state points to maximize performance at the design point. In addition, the paper also presented a method to optimize the performance of the Rankine cycle. A novelty of this method is the selection of four different approaches to control the cycle. Both methods follow a novel equation-oriented approach enabling the use of an efficient gradient-based optimization algorithm. This means that the underlying Rankine cycle model doesn't have to be solved at each intermediate optimization iteration which reduces the computational cost.

The capabilities of the proposed methods were demonstrated through a case study for power generation from the batch-wise casting process at a representative ferroalloy plant. More specifically the proposed methods were used to design and analyze three Rankine cycles with CO_2 as the working fluid. The main results from the case study are the following:

- The design optimization problem contains few local optimums, and the design optimization method converges to the global optimum with a high probability regardless of the starting point used for optimization.
- The "VRS and VIGV" control approach yield the largest annual electricity production of 12.6 GWh.
- The VRS control approach yields up to 9.2% larger annual electricity production than the sliding pressure control approach due to the increased RIT off-design efficiency.
- The VIGV control approach yields up to 10.5% larger annual electricity production than the sliding pressure control approach due to the facilitation of operating at larger working fluid pressures.
- The sliding pressure control approach performed best for the Rankine cycle where the RIT and the HXs were designed for optimal performance at an average operating condition. This Rankine cycle operated closer to its design point than the other designs.

Considering the flexibility, robustness and the computational cost of the proposed methods, they can be regarded as a powerful tool for the preliminary design and performance prediction of Rankine cycles.

Credit author statement

Brede A. L. Hagen: Methodology, Software, Formal analysis, Writing – original draft, Writing – review & editing, Visualization, Trond Andresen: Formal analysis, Writing – review & editing, Visualization, Petter Nekså; : Writing – review & editing, Supervision

Declaration of competing interest

The authors declare that they have no known competing financial interests or personal relationships that could have appeared to influence the work reported in this paper.

Acknowledgments

This publication has been funded by HighEFF - Centre for an Energy Efficient and Competitive Industry for the Future, an 8-years' Research Centre under the FME-scheme (Centre for Environment-friendly Energy Research, 257632). The authors gratefully acknowledge the financial support from the Research Council of Norway and user partners of HighEFF.

References

[1] An official website of the Eurpean Union [Online]. Available: https://ec.europa.eu/clima/policies/strategies/2030_en. [Accessed 16 July 2021].
[2] Tian H, Shu GQ. Organic Rankine Cycle systems for large-scale waste heat recovery to produce electricity. In: Macchi E, Astolfi M, editors. Organic Rankine cycle (ORC) power systems: technologies and applications. Woodhead Publishing; 2017. p. 613–36.
[3] Guercio A, Bini R. Biomass-fired Organic Rankine Cycle combined heat and power systems. In: Macchi E, Astolfi M, editors. Organic Rankine cycle (ORC) power systems: technologies and applications. Woodhead Publishing; 2017. p. 527–67.
[4] Orosz M, Dickes R. Solar thermal powered organic Rankine cycles. In: Macchi E, Astolfi M, editors. Organic Rankine cycle (ORC) power systems: technologies and applications. Woodhead Publishing; 2017. p. 569–612.
[5] Spadacini C, Xodo LG, Quaia M. Geothermal energy exploitation with organic Rankine cycle technologies. In: Macchi E, Astolfi M, editors. Organic Rankine cycle (ORC) power systems: technologies and applications. Woodhead Publishing; 2017. p. 473–525.
[6] Tchanche BF, Pétrissans M, Papadakis G. Heat resources and organic Rankine cycle machines. Renew Sustain Energy Rev 2014;39:1185–99.
[7] Gülen SC. Steam turbine—Quo Vadis? Front Energy Res 2021;8:1–20. February.
[8] Colonna P, et al. Organic Rankine cycle power systems: from the concept to current technology, applications, and an outlook to the future. J Eng Gas Turbines Power 2015;137(10):1–19.
[9] Macchi E. Theoretical basis of the organic Rankine cycle. In: Macchi E, Astolfi M, editors. Organic Rankine cycle (ORC) power systems: technologies and applications. Woodhead Publishing; 2017. p. 3–24.
[10] Brun K, Friedman P, Dennis R. Fundamentals and applications of supercritical carbon dioxide (sCO_2) based power cycles. Woodhead Publishing; 2017.
[11] Capra F, Martelli E. Numerical optimization of combined heat and power Organic Rankine Cycles – Part B: simultaneous design & part-load optimization. Energy Oct. 2015;90:329–43.
[12] Martelli E, Capra F, Consonni S. Numerical optimization of combined heat and power organic Rankine cycles – Part A: design optimization. Energy 2015;90:310–28. Oct.

[13] Quoilin S, Aumann R, Grill A, Schuster A, Lemort V, Spliethoff H. Dynamic modeling and optimal control strategy of waste heat recovery Organic Rankine Cycles. Appl Energy 2011;88(6):2183–90.
[14] Schuster S, Markides CN, White AJ. Design and off-design optimisation of an organic Rankine cycle (ORC) system with an integrated radial turbine model. Appl Therm Eng 2020;174:115192. Jun.
[15] Dong S, Hu X, Huang JF, Zhu T, Zhang Y, Li X. Investigation on improvement potential of ORC system off-design performance by expander speed regulation based on theoretical and experimental exergy-energy analyses. Energy 2021;220:119753.
[16] Bahamonde S, Pini M, De Servi C, Rubino A, Colonna P. Method for the preliminary fluid dynamic design of high-temperature mini-organic Rankine cycle turbines. J Eng Gas Turbines Power 2017;139(8):1–14.
[17] Valdimarsson P. Radial inflow turbines for organic Rankine cycle systems. In: Macchi E, Astolfi M, editors. Organic Rankine cycle (ORC) power systems: technologies and applications. Woodhead Publishing; 2017. p. 321–34.
[18] Moustapha H, Zelesky MF, Baines NC, Japikse D. Axial and radial turbines. USA: Concepts NREC; 2003. Vermont.
[19] Spence SW, Artt DW. Experimental performance evaluation of a 99.0 mm radial in flow nozzled turbine with different stator throat areas. In: Proceedings of the institution of mechanical engineers, Part A: journal of power and energy, vol. 211; 1997. p. 477–88.
[20] Spence SWT, Doran WJ, Artt DW. Experimental performance evaluation of a 99.0 mm radial inflow nozzled turbine at larger stator-rotor throat area ratios. Proc Inst Mech Eng Part A J Power Energy 1999;213(3):205–18.
[21] Hagen BAL, Agromayor R, Nekså P. Equation-oriented methods for design optimization and performance analysis of radial inflow turbines. Energy 2021;237(121596).
[22] Hu D, Li S, Zheng Y, Wang J, Dai Y. Preliminary design and off-design performance analysis of an Organic Rankine Cycle for geothermal sources. Energy Convers Manag 2015;96:175–87. May.
[23] Zhai L, et al. An improved modeling for low-grade organic Rankine cycle coupled with optimization design of radial-inflow turbine. Energy Convers Manag 2017;153:60–70.
[24] Palagi L, Sciubba E, Tocci L. A neural network approach to the combined multi-objective optimization of the thermodynamic cycle and the radial inflow turbine for Organic Rankine cycle applications. Appl Energy 2019;237:210–26.
[25] Du Y, Chen K, Dai Y. A study of the optimal control approach for a Kalina cycle system using a radial-inflow turbine with variable nozzles at off-design conditions. Appl Therm Eng 2019;149:1008–22. Feb.
[26] Song J, et al. Thermodynamic and economic investigations of transcritical CO2-cycle systems with integrated radial-inflow turbine performance predictions. Appl Therm Eng 2020;165.
[27] Yao L, Zou Z. A one-dimensional design methodology for supercritical carbon dioxide Brayton cycles: integration of cycle conceptual design and components preliminary design. Appl Energy 2020;276:115354. March.
[28] Li Y, Li W, Gao X, Ling X. Thermodynamic analysis and optimization of organic Rankine cycles based on radial-inflow turbine design. Appl Therm Eng 2021;184:116277. November 2020.
[29] Walnum HT, Nekså P, Nord LO, Andresen T. Modelling and simulation of CO2 (carbon dioxide) bottoming cycles for offshore oil and gas installations at design and off-design conditions. Energy 2013;59:513–20. Sep.
[30] Hagen BAL, Nikolaisen M, Andresen T. A novel methodology for Rankine cycle analysis with generic heat exchanger models. Appl Therm Eng 2020;165.
[31] Gnielinski V. New equations for heat and mass transfer in turbulent pipe and channel flow. Int Chem Eng 1976;16(2):359–68.
[32] Selander WN. Explicit formulas for the computation of friction factors in turbulent pipe flow. 1978.
[33] Shah MM. A general correlation for heat transfer during film condensation inside pipes. Int J Heat Mass Tran 1979;22(4):547–56.
[34] Friedel L. Improved friction pressure drop correlation for horizontal and vertical two-phase pipe flow. In: European two-phase flow group meeting; 1979.
[35] Incropera FP, Dewitt DP, Bergman TL, Lavine AS. Fundamentals of heat and mass transfer. sixth ed. John Wiley & Sons; 2006.
[36] Lemmon EW, Bell IH, Huber ML, McLinden MO. NIST standard reference database 23: reference fluid thermodynamic and transport properties-REFPROP, Version 10.0. National Institute of Standards and Technology; 2018.
[37] Aungier RH. Turbine aerodynamics: axial-flow and radial-inflow turbine design and analysis. New York: ASME Press; 2005.
[38] Schittkowski K. NLPQL: a FORTRAN subroutine solving constrained nonlinear programming problems. Ann Oper Res 1985;5(1–4):485–500.
[39] Astolfi M, Martelli E, Pierobon L. Thermodynamic and technoeconomic optimization of organic Rankine cycle systems. In: Macchi E, Astolfi M, editors. Organic Rankine cycle (ORC) power systems. Woodhead Publishing; 2017. p. 173–249.
[40] Pili R, García Martínez L, Wieland C, Spliethoff H. Techno-economic potential of waste heat recovery from German energy-intensive industry with Organic Rankine Cycle technology. Renew Sustain Energy Rev 2020;134:110324. February.
[41] Børset MT. Energy dissipation and recovery in the context of silicon production. PhD thesis. NTNU; 2015.
[42] Andresen T, Lingaas S, Hagen BAL, Nekså P. Dynamic analysis of energy recovery utilizing thermal storage from batch-wise metal casting. In: Rankine 2020 conference; 2020.
[43] Invernizzi CM, Bonalumi D. Thermal stability of organic fluids for Organic Rankine Cycle systems. In: Macchi E, Astolfi M, editors. Organic Rankine cycle (ORC) power systems: technologies and applications. Woodhead Publishing; 2017. p. 121–51.
[44] White MT, Bianchi G, Chai L, Tassou SA, Sayma AI. Review of supercritical CO2 technologies and systems for power generation. Appl Therm Eng 2021;185.
[45] Musgrove G, Sullivan S, Shiferaw D, Fourspring P, Chordia L. Heat exchangers," in *Fundamentals and Applications of supercritical carbon dioxide (SCO2) based power cycles*. Woodhead Publishing; 2017. p. 217–44.
[46] Uusitalo A, Ameli A, Turunen-Saaresti T. Thermodynamic and turbomachinery design analysis of supercritical Brayton cycles for exhaust gas heat recovery. Energy 2019;167:60–79.